Topological Crystalline Insulator Phase in Graphene Multilayers

M. Kindermann

Phys. Rev. Lett. **114**, 226802 — Published 2 June 2015

DOI: 10.1103/PhysRevLett.114.226802

Topological crystalline insulator phase in graphene multilayers

M. Kindermann
School of Physics, Georgia Institute of Technology, Atlanta, Georgia 30332, USA

While the experimental progress on three dimensional topological insulators is rapid, the development of their 2D counterparts has been comparatively slow, despite their technological promise. The main reason is materials challenges of the to date only realizations of 2D topological insulators, in semiconductor quantum wells. Here we identify a 2D topological insulator in a material which does not face similar challenges and which is by now most widely available and well-charaterized: graphene. For certain commensurate interlayer twists graphene multilayers are insulators with sizable bandgaps. We show that they are moreover in a topological phase protected by crystal symmetry. As its fundamental signature, this topological state supports one-dimensional boundary modes. They form low-dissipation quantum wires that can be defined purely electrostatically.

PACS numbers: 73.22.Pr,73.21.Ac,73.43.-f,72.80.Vp

There are physical systems with properties that depend only on global topology, but not on local details. Because of their inherent stability against perturbations systems in such topological phases have attracted much interest, both from a fundamental and a technological point of view. The first topological phase realized in a condensed matter system was the quantum Hall state, which occurs in two-dimensional (2D) electron gases subject to a strong magnetic field. Rather recently a new class of such systems has been discovered: topological insulators (TI) [1–3]. These materials typically have strong spin-orbit interactions and their topological character invokes time-reversal symmetry. Later, also topological phases protected by crystal symmetries, such as mirror symmetry [4–10], have been predicted and observed, so-called topological crystalline insulators (TCI) [11–13].

The experimental activity in the field so far has focused on three-dimensional systems, although TIs in two dimensions enjoy a number of advantages. For example, bulk charge carriers that pose a major experimental challenge for their three-dimensional counterparts can be eliminated easily by gating. Nevertheless, experimental progress on 2D TIs to date is hampered by materials challenges. The only 2D TI realized so far is the quantum spin Hall (QSH) state [3] induced by spin-orbit interaction and characterized by pairs of time-reversed boundary modes, so-called helical edge states. This state was predicted to occur in graphene [14, 15], HgTe and InAs/GaSb quantum wells [16, 17], and several other 2D materials [18–20]. It was observed in milestone experiments on HgTe [21] and later in InAs/GaSb [22]. Subsequent research activity, however, has been limited due to experimental challenges specific to these material systems. Graphene does not pose those challenges and it is a by now most widely available and investigated material. From this point of view it appears to be the ideal system to implement 2D TI states. However, unfortunately the spin-orbit coupling in graphene is too weak [23, 24] to observe the QSH phase as originally predicted [14] in present day experiments. This has motivated much subsequent research on how to drive graphene into a stable topological phase by many-body interactions [25–28], radiation [29], or enhanced spin-orbit interaction [30–37].

In this Letter we propose an alternate route to inducing topological phases in graphene: utilizing the interlayer coupling in twisted graphene multilayers. For graphene bilayers with a commensurate interlayer twist Mele has demonstrated [38] that the interlayer interaction can open sizable spectral gaps when the sublattice exchange (SE) symmetry is preserved. Here we show that at low energies the resulting state is a mirror TCI, a topological phase distinct from the QSH insulator, requiring neither spin-orbit interactions nor time-reversal symmetry. It is protected by robust gaps, predicted to reach the order of ten meV [38, 39]. Invoking a crystal symmetry rather than time-reversal symmetry, the proposed TCI and its edge modes are vulnerable to potential disorder, different from strong TIs. However, as in strong TIs, gapless boundary excitations can be observed in any crystallographic direction. This is in contrast to generic TCIs that have gapless modes only in high-symmetry directions or planes.

Model : We first consider a graphene bilayer with even SE symmetry and spinless electrons, as depicted in Fig. 1. The low-energy theory of such a bilayer was derived by Mele in Ref. [38] and it can be written as

$$H = v\left(p_S\sigma_x\tau_z + p_{\bar{S}}\sigma_y\right) + \gamma e^{i\theta l_z\sigma_z\tau_z} l_x e^{-i\theta l_z\sigma_z\tau_z} \qquad (1)$$

[54]. Here, $\boldsymbol{p} = \boldsymbol{\nabla}/i$ (we set $\hbar = 1$) is the electron momentum with components p_S along the mirror axis S in Fig. 1 and $p_{\bar{S}}$ in the direction perpendicular to it. Furthermore, v is the charge carrier velocity in graphene, and γ and θ parametrize the low-energy interlayer coupling due to lattice commensuration [38]. The Pauli matrices σ_i act on the pseudospin of graphene, which distinguishes the two sublattices A and B [40]: electrons with pseudospin-up reside on sublattice A and those with pseudospin-down correspondingly on sublattice B. The Pauli matrices τ_i act on the "valley spin," which is up in band structure valley K and down in valley K'. Also

the l_i are Pauli marices and they act on a "layer spin," with spin-up on the top layer and layer spin-down on the lower one. We disregard the electron spin for now.

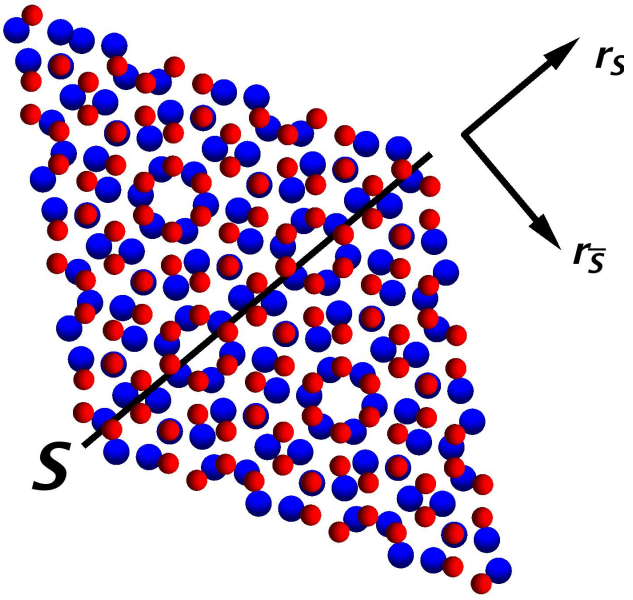

FIG. 1: (color online). SE-even graphene bilayer with an interlayer twist angle of 38.213°. The structure has C_2-symmetry on S. For clarity the top layer atoms are depicted smaller than those in the lower layer.

Symmeries and Topological Classification:

The first ingredient to the symmetry that protects [11] the topological phase proposed here is $\mathcal{M}$, a C_2 symmetry at the axis S in Fig. 1. From a strictly 2D viewpoint, $\mathcal{M}$ is a combined mirror and interlayer symmetry: mirror reflection on S and simultaneous layer interchange leaves an SE-even graphene bilayer unchanged. In the above notation the symmetry $\mathcal{M}$ has the form

$$\mathcal{M} = M l_x \sigma_x, \tag{2}$$

where M denotes mirror reflection on S of the spatial coordinates: $M\,(r_S, r_{\bar{S}}) = (r_S, -r_{\bar{S}})$, cf. Fig. 1.

The second ingredient is a chiral symmetry

$$\tilde{\Sigma} = l_z \sigma_z, \tag{3}$$

which is due to the particle-hole symmetry of the low-energy theory of the system. One readily checks that one has indeed $\{H, \tilde{\Sigma}\} = 0$ for the H of Eq. (1). We show below that in the space of Hamiltonians h that have the combined chiral and reflection symmetry

$$\Sigma = \tilde{\Sigma}\mathcal{M}, \tag{4}$$

that is $\{h, \Sigma\} = 0$, the above Hamiltonian H indeed is topologically nontrivial. Within the classification scheme of Ref. [41], the SE-even graphene bilayer thus is an $M\mathbb{Z}$-mirror TCI of class BDI. When time-reversal symmetry is broken by extra, Σ-symmetric terms it is of class AIII.

Topological Invariant: The topological arguments below are formulated for lattice models, building on their periodicity in momentum space. For the purposes of that discussion we therefore analyze a lattice model that has the same low-energy Hamiltonian Eq. (1) as an SE-even graphene bilayer, but that has in addition an exact chiral symmetry $\tilde{\Sigma}$ (not only one at low energies): a tight-binding model of a commensurately rotated graphene bilayer as typically assumed [42], but with interlayer hopping only between equal sublattices (A-to-A and B-to-B). As shown below, the SE-even graphene bilayer inherits its topological properties from that model.

The nontrivial topology of this lattice model is characterized by the integer invariant [41, 43]

$$N_1 = \frac{1}{4\pi i} \int_{\mathrm{sBZ}} dp_S \,\mathrm{tr}\, \Sigma H^{-1} \partial_{p_S} H \Big|_{p_{\bar{S}}=0}. \tag{5}$$

Here, ∂_α denotes the partial derivative with respect to α and the trace tr runs over all sites of the supercell defined by the lattice commensuration. Symmetry under translations by supercell lattice vectors is assumed and p_S, $p_{\bar{S}}$ are the Bloch momentum eigenvalues in the specified directions. The integration in Eq. (5) is along the line $p_{\bar{S}} = 0$ of mirror symmetric momenta. It covers one period in the Brillouin zone of the supercell (sBZ). An explicit calculation shows that in our model $N_1 = 2\,\mathrm{sgn}(\gamma \sin 2\theta)$, where $\mathrm{sgn}\, x$ is the sign of x (cf. supplementary material A). The integer nature of the above invariant is born out by an extension of our model to SE-even graphene multi-layers. For a $2N$-layer as defined in supplementary material A and with an appropriately generalized chiral symmetry one then finds $N_1 = 2N\mathrm{sgn}(\gamma \sin 2\theta)$.

Index Theorem and Boundary Modes: The fundamental signature of topological phases are ungapped modes at boundaries between topologically distinct regions. For the mirror TCI of class BDI in two dimensions there is an index theorem [43–45] that relates n_Σ, the sum over the Σ-eigenvalues of all boundary modes at momentum $p_{\bar{S}} = 0$, to the difference between the invariants $N_1^{(l)}$ and $N_1^{(r)}$ left and right of a boundary, respectively:

$$n_\Sigma = N_1^{(r)} - N_1^{(l)}. \tag{6}$$

It implies a lower bound $|N_1^{(r)} - N_1^{(l)}|$ on the number of boundary modes between regions with differing topological invariants [55].

In particular at edges, the boundary to the topologically trivial vacuum state with $N_1 = 0$, such modes can appear. This occurs when an edge respects the symmetry $\mathcal{M}$, that is for edges perpendicular to S. According the index theorem Eq. (6) there are at least two boundary

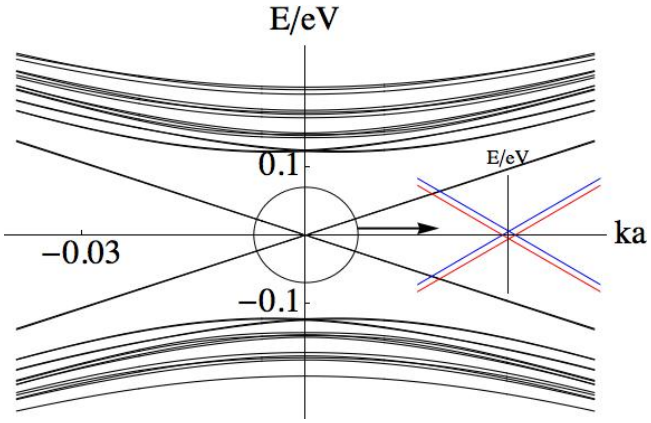

FIG. 2: (color online). Spectrum of a 60 unit cells wide ribbon implementing the lattice model described in the main text at an interlayer rotation angle of 38.213°. Here, the edges are perpendicular to the axis S in Fig. 1, so as to preserve $\mathcal{M}$-symmetry. Two degenerate pairs of edge modes are demonstrated, one pair per edge. In the zoom into the low-energy region shown in the inset the two pairs of modes are depicted with an (artificial) energy offset. Momentum is measured in units of $1/a$, the inverse lattice constant of graphene.

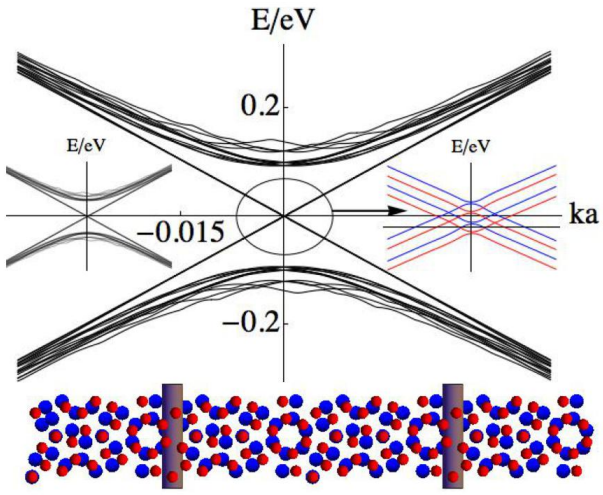

FIG. 3: (color online). Spectrum of a ribbon of the same width as in Fig. 2, but in the perpendicular crystallographic direction. Periodic boundary conditions are applied and two flux tubes parallel to S, each inducing a sign change in the interlayer coupling γ, are inserted. The flux tubes (gray cylinders in the lattice cartoon picture of the lower panel) break $\mathcal{M}$-symmetry on the lattice scale, yet four topological boundary modes per flux tube are observed (momentum is measured relative to the K-points; states from both K-points are shown). Inset (right): Zoom into the low-energy region with an (artificial) energy offset for different modes. Inset (left): The same spectrum for a ribbon with additional pseudospin off-diagonal interlayer hopping (A - to - B and B - to - A), as in bilayer graphene. The same boundary modes are observed.

modes at such an edge. These gapless modes are clearly observed in the spectrum of an $\mathcal{M}$-symmetric ribbon that implements the above bilayer lattice model, cf. Fig. 2.

The line $p_{\bar{S}} = 0$ cuts through the K-points of graphene and the topological charge of Eq. (5) is concentrated around those points (cf. supplementary material A). The low-energy theory Eq. (1) thus inherits its topological properties from the above lattice model. Consequently, also SE-even bilayer graphene at low energies, which is described by Eq. (1), has the invariant N_1 and the predicted boundary modes. Outside the low-energy regime described by Eq. (1), the pseudo spin off-diagonal interlayer coupling in SE-even bilayer graphene (A - to - B and B - to - A) may break the chiral symmetry $\tilde{\Sigma}$. The topological modes then disappear. This may happen in the presence of short wavelength perturbations such as abrupt edges. The zero modes in Fig. 2 thus become gapped upon inclusion of off-diagonal interlayer hopping.

Gapless boundary modes in SE-even bilayer graphene can be observed in systems with smoothly space-dependent parameters. For example, a sign change of N_1 with accompanying boundary modes could in principle be induced by the threading of half a magnetic flux quantum through a tube in the gap between the two layers. We demonstrate the predicted four boundary modes per flux tube in Fig. 3 for a ribbon with two such tubes. To avoid additional edge modes here periodic boundary conditions are applied. While the main panel of Fig. 3 is made for our above, exactly $\tilde{\Sigma}$-symmetric model, the inset shows the spectrum of the same ribbon when pseudo spin off-diagonal interlayer hopping is included, as in SE-even bilayer graphene. The same eight boundary modes are found, confirming that the low-energy theory of SE-even bilayer graphene indeed inherits its topological structure from the above model.

Because of its rotational invariance, the low-energy Hamiltonian Eq. (1) has a topological invariant N_1 not only in the presence of mirror symmetry on S, but also for any other mirror axis (with appropriately rotated chiral symmetry Σ' and line of integration through momentum space). Interestingly, one therefore expects that topologically protected gapless modes can appear along any crystallographic direction, not just in high-symmetry directions as in generic TCIs. In the ribbon of Fig. 3 the inserted flux tubes are parallel to S and they thus break $\mathcal{M}$-symmetry on the lattice scale. Nevertheless, eight gapless modes are observed, a first confirmation of this unusual property. We have verified this for flux tubes in a number of other crystallographic directions, all of which exhibit the predicted zero modes. Two more examples are demonstrated in Fig. 4, which shows the spectra of ribbons with flux tubes at angles 23.4° and 8.7° with respect to S. The direction of the inserted flux tubes relative to the lattice and the evolution of the observed zero modes with increasing interlayer coupling are shown in Figs. 6 and 7 of supplementary material A.

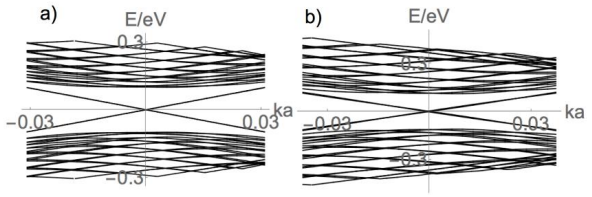

FIG. 4: Spectra as in Fig. 3 for a ribbon with flux tubes at angles 23.4° (a) and 8.7° (b) with S. Due to the rotational invariance of Eq. (1) zero modes are again observed, although the flux tubes break $\mathcal{M}$ on the lattice scale.

The same boundary modes can also be observed in an experimentally much more accessible set-up: an SE-even graphene bilayer subject to an electric potential V, which is constant along a line l, but confined to within a small distance $w \ll v/\Delta$ from l. Here, $\Delta = 2\gamma \sin 2\theta$ is the spectral gap of the Hamiltonian (1). The potential V has mirror symmetry on lines $\tilde{S}$ perpendicular to l and due to its rotation symmetry the Hamiltonian can be brought into the form of Eq. (1) with r_S and $r_{\bar{S}}$ replaced by the coordinates $r_{\tilde{S}}$ and $r_{\bar{\tilde{S}}}$ parallel and perpendicular to $\tilde{S}$, respectively. We then eliminate V by the transformation

$$U(r_{\tilde{S}}) = e^{-i\phi(r_{\tilde{S}})\sigma_x\tau_z}, \tag{7}$$

where $\phi(r_{\tilde{S}}) = \int_{-\infty}^{r_{\tilde{S}}} dr'_{\tilde{S}}\, V(r'_{\tilde{S}})$, at the expense of a modified interlayer coupling term in the transformed Hamiltonian $U^\dagger H U$. One finds that if the total phase $\phi(\infty)$ that electrons acquire in the potential V is an integer multiple of $\pi/2$ then far from l the interlayer Hamiltonian after the transformation still has the form of Eq. (1). However, if $\phi(\infty)$ is an odd integer multiple of $\pi/2$ then in the transformed Hamiltonian the sign of θ to the left of l differs from the one to the right of l. Consequently N_1 changes sign across l and at least four boundary modes appear according to Eq. (6). Close to l, where V is nonzero, there is an extra term $\Delta \sin(2\phi)\Sigma M/2$ in the transformed Hamiltonian, which breaks the chiral symmetry Σ. However, while the maximum of that perturbation is of the order of the gap Δ, at $w \ll v/\Delta$ it is appreciable only in a region narrow on the scale of the spatial extent of the boundary modes. Therefore the resulting perturbation of the boundary mode energies is small compared to Δ and in the limit $w\Delta/v \to 0$ these modes are still gapless. In Fig. 5 we demonstrate these modes numerically.

Graphene multilayers with interlayer twist occur naturally when grown on certain substrates [46, 47], or can be manufactured by stacking graphene single-layers [48]. To observe the predicted effects the twist angle needs not to be exactly commensurate, but only near a commensuration [49], e.g. within $\simeq 0.1°$ degrees of 38.213° [56]. Extraordinary control of the twist angles between graphene layers has already been demonstrated in experiments [50], bringing the predicted physics into experimental reach. The described line potential can be created by a pair of

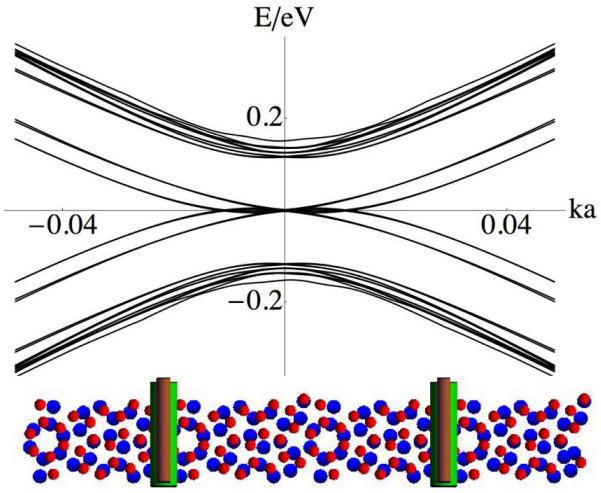

FIG. 5: (color online). Spectrum of the same ribbon as shown in Fig. 3, but with the flux tubes replaced by two line potentials, generated by pairs of oppositely charged wires (brown and green cylinders in the lattice cartoon of the lower panel).

of oppositely charged wires, such as carbon nanotubes, at distance of order w from one another and the sample.

We point out that the TCI phase discussed here is distinct from so-called marginal topological states, such as in biased Bernal stacked graphene bilayers [51, 52]. The topological winding numbers in the latter states are nonzero only in either of the two band structure valleys separately. When adding up the contributions from both valleys they cancel. In the TCI phase considered here, however, they add up to a nonzero integer. In contrast with the state of Ref. [52], the TCI phase discussed here therefore is robust against Σ-preserving intervalley scattering, as demonstrated in supplementary material B. There it moreover is shown that the predicted topological state is robust against the intrinsic spin-orbit coupling of graphene and an interlayer bias.

Conclusion: Our discussion identifies a 2D TCI in a most widely available material system: graphene multilayers. Interestingly and atypically for TCIs, topological boundary modes can be induced in arbitrary spatial directions. From an experimental point of view, graphene does not pose the challenges of previous implementations of 2D TIs in semiconductor heterostructures. It moreover is accessible to a number of powerful experimental probes not available for such heterostructures, such as scanning tunneling microscopy and angle resolved photoemission spectroscopy. It can therefore be hoped that this proposal will significantly advance the development of 2D TIs with their exciting applications.

The author thanks L. Fu, P. M. Goldbart, P. Jarillo-Herrero, E. J. Mele, and J. Sanchez-Yamagishi for discussions and gratefully acknowledges financial support from the NSF (DMR-1055799).

[1] J. E. Moore, Nature **464**, 194 (2010).
[2] M. Z. Hasan and C. L. Kane, Rev. Mod. Phys. **82**, 3045 (2010).
[3] X.-L. Qi and S.-C. Zhang, Rev. Mod. Phys. **83**, 1057 (2011).
[4] T. H. Hsieh, H. Lin, J. Liu, W. Duan, A. Bansil, and L. Fu, Nat. Comm. **3**, 982 (2012).
[5] Y. Tanaka, Z. Ren, T. Sato, K. Nakayama, S. Souma, T. Takahashi, K. Segawa, and Y. Ando, Nat. Phys. **8**, 800 (2012).
[6] P. Dziawa, B. J. Kowalski, K. Dybko, R. Buczko, A. Szczerbakow, M. Szot, E. Łusakowska, T. Balasubramanian, B. M. Wojek, M. H. Berntsen, et al., Nat. Mater. **11**, 1023 (2012).
[7] S.-Y. Xu, C. Liu, N. Alidoust, D. Qian, M. Neupane, J. D. Denlinger, Y. J. Wang, L. A. Wray, R. J. Cava, H. Lin, et al. (2012), 1206.2088.
[8] H. Yao and S. Ryu (2012), 1202.5805.
[9] S.-Y. Xu, C. Liu, N. Alidoust, M. Neupane, D. Qian, I. Belopolski, J. D. Denlinger, Y. J. Wang, H. Lin, L. A. Wray, et al., Nat. Comm. **3**, 1192 (2012).
[10] F. Zhang, C. L. Kane, and E. J. Mele (2013), 1303.4144.
[11] Y. Ando and L. Fu, Annual Review of Condensed Matter Physics **6**, 361 (2015).
[12] L. Fu, Phys. Rev. Lett. **106**, 106802 (2011).
[13] R.-J. Slager, A. Mesaros, V. Juricic, and J. Zaanen, Nat. Phys. **9**, 98 (2013).
[14] C. L. Kane and E. J. Mele, Phys. Rev. Lett. **95**, 226801 (2005).
[15] C. L. Kane and E. J. Mele, Phys. Rev. Lett. **95**, 146802 (2005).
[16] B. A. Bernevig, T. L. Hughes, and S.-C. Zhang, Science **314**, 1757 (2006).
[17] C. Liu, T. L. Hughes, X.-L. Qi, K. Wang, and S.-C. Zhang, Phys. Rev. Lett. **100**, 236601 (2008).
[18] S. Murakami, Phys. Rev. Lett. **97**, 236805 (2006).
[19] D. Xiao, W. Zhu, Y. Ran, N. Nagaosa, and S. Okamoto, Nat. Comm. **2**, 596 (2011).
[20] P. Ghaemi, S. Gopalakrishnan, and T. L. Hughes, Phys. Rev. B **86**, 201406 (2012).
[21] M. König, S. Wiedmann, C. Brüne, A. Roth, H. Buhmann, L. W. Molenkamp, X.-L. Qi, and S.-C. Zhang, Science **318**, 766 (2007).
[22] I. Knez, R.-R. Du, and G. Sullivan, Phys. Rev. Lett. **107**, 136603 (2011).
[23] Y. Yao, F. Ye, X.-L. Qi, S.-C. Zhang, and Z. Fang, Phys. Rev. B **75**, 041401 (2007).
[24] J. C. Boettger and S. B. Trickey, Phys. Rev. B **75**, 121402 (2007).
[25] S. Raghu, X.-L. Qi, C. Honerkamp, and S.-C. Zhang, Phys. Rev. Lett. **100**, 156401 (2008).
[26] C. Weeks and M. Franz, Phys. Rev. B **81**, 085105 (2010).
[27] F. Zhang, J. Jung, G. A. Fiete, Q. Niu, and A. H. MacDonald, Phys. Rev. Lett. **106**, 156801 (2011).
[28] T. Pereg-Barnea and G. Refael, Phys. Rev. B **85**, 075127 (2012).
[29] V. G. Netanel H. Lindner, Gil Refael, Nat. Phys. **7**, 490 (2011).
[30] A. Varykhalov, J. Sánchez-Barriga, A. M. Shikin, C. Biswas, E. Vescovo, A. Rybkin, D. Marchenko, and O. Rader, Phys. Rev. Lett. **101**, 157601 (2008).
[31] A. H. Castro Neto and F. Guinea, Phys. Rev. Lett. **103**, 026804 (2009).
[32] S. Abdelouahed, A. Ernst, J. Henk, I. V. Maznichenko, and I. Mertig, Phys. Rev. B **82**, 125424 (2010).
[33] C. Weeks, J. Hu, J. Alicea, M. Franz, and R. Wu, Phys. Rev. X **1**, 021001 (2011).
[34] Z. Qiao, W.-K. Tse, H. Jiang, Y. Yao, and Q. Niu, Phys. Rev. Lett. **107**, 256801 (2011).
[35] H. Jiang, Z. Qiao, H. Liu, J. Shi, and Q. Niu, Phys. Rev. Lett. **109**, 116803 (2012).
[36] J. Hu, J. Alicea, R. Wu, and M. Franz, Phys. Rev. Lett. **109**, 266801 (2012).
[37] Z. Qiao, X. Li, W.-K. Tse, H. Jiang, Y. Yao, and Q. Niu, Phys. Rev. B **87**, 125405 (2013).
[38] E. J. Mele, Phys. Rev. B **81**, 161405 (2010).
[39] S. Shallcross, S. Sharma, and O. A. Pankratov, Phys. Rev. Lett. **101**, 056803 (2008).
[40] A. H. Castro Neto, F. Guinea, N. M. R. Peres, K. S. Novoselov, and A. K. Geim, Rev. Mod. Phys. **81**, 109 (2009).
[41] C.-K. Chiu, H. Yao, and S. Ryu, arXiv:1303.1843 (2013).
[42] S. Reich, J. Maultzsch, C. Thomsen, and P. Ordejón, Phys. Rev. B **66**, 035412 (2002).
[43] A. M. Essin and V. Gurarie, Phys. Rev. B **84**, 125132 (2011).
[44] E. J. Weinberg, Phys. Rev. D **24**, 2669 (1981).
[45] G. E. Volovik, *The Universe in a Helium Droplet*, vol. Chapter 22 (Clarendon, Oxford, 2003).
[46] C. Berger, Z. Song, T. Li, X. Li, A. Y. Ogbazghi, R. Feng, Z. Dai, A. N. Marchenkov, E. H. Conrad, P. N. First, et al., J. Phys. Chem. B **108**, 19912 (2004).
[47] W. Yan, M. Liu, R.-F. Dou, L. Meng, L. Feng, Z.-D. Chu, Y. Zhang, Z. Liu, J.-C. Nie, and L. He, Phys. Rev. Lett. **109**, 126801 (2012).
[48] J. D. Sanchez-Yamagishi, T. Taychatanapat, K. Watanabe, T. Taniguchi, A. Yacoby, and P. Jarillo-Herrero, Phys. Rev. Lett. **108**, 076601 (2012).
[49] H. K. Pal, S. Carter, and M. Kindermann, arXiv:1409.1971 (2014).
[50] A. Mishchenko, J. S. Tu, Y. Cao, R. V. Gorbachev, J. R. Wallbank, M. T. Greenaway, V. E. Morozov, S. V. Morozov, M. J. Zhu, S. L. Wong, et al., Nat Nano **9**, 808 (2014).
[51] J. Li, A. F. Morpurgo, M. Büttiker, and I. Martin, Phys. Rev. B **82**, 245404 (2010).
[52] I. Martin, Y. M. Blanter, and A. F. Morpurgo, Phys. Rev. Lett. **100**, 036804 (2008).
[53] J. M. B. Lopes dos Santos, N. M. R. Peres, and A. H. Castro Neto, Phys. Rev. Lett. **99**, 256802 (2007).
[54] At high energies there are additional interlayer coupling terms that do not conserve the "Dirac" momentum $\boldsymbol{p}$ that appears in Eq. (1) [53]. At the (large) interlayer rotation angles of interest here, however, these terms merely renormalize the carrier velocity v [53] in the low-energy theory Eq. (1) and they thus do not appear explicitly.
[55] Pairs of boundary modes with opposite Σ eigenvalues evidently do not contribute to n_Σ and can increase the number of boundary modes above $|N_1^{(r)} - N_1^{(l)}|$.
[56] In a graphene bilayer rotated by angle $\delta\varphi$ from a commensurate angle φ, regions with size of the order $a/\delta\varphi$ appear, that have approximately SE-even stacking. There the described topological modes can be observed if their spatial extent v/Δ is smaller than those regions. For

$\varphi = 38.213^\circ$ with $\Delta \simeq 10$meV [39] this is fulfilled when $\delta\varphi \simeq 0.1^\circ$.